
PROPENSITY OF WATER SELF-IONS AT AIR(OIL)-WATER INTERFACES REVEALED BY DEEP POTENTIAL MOLECULAR DYNAMICS WITH ENHANCED SAMPLING

Pengchao Zhang¹, Axel Tosello Gardini^{2,3}, and Xuefei Xu^{1,*}.

¹Center for Combustion Energy, Department of Energy and Power Engineering, and Key Laboratory for Thermal Science and Power Engineering of Ministry of Education, Tsinghua University, Beijing 100084, China

²Atomistic Simulations, Italian Institute of Technology, Genova 16152, Italy

³Department of Materials Science, Università di Milano-Bicocca, 20126 Milano, Italy

*Corresponding author e-mail: xuxuefei@tsinghua.edu.cn

ABSTRACT

The preference of water self-ions (hydronium and hydroxide) near air/oil-water interfaces is one of the hottest topics in water research due to its importance for understanding properties, phenomena, and reactions of interfaces. In this work, we performed enhanced-sampling molecular dynamics based on state-of-the-art neural network potentials with M06-2X accuracy to investigate the propensity of hydronium and hydroxide ions at air/oil-water interfaces, which can simultaneously describe well the water autoionization process forming these ions, recombination of ions, and ionic distribution along the normal distance to the interface by employing a set of appropriate Voronoi collective variables. The results support a stable ionic double-layer distribution near the interface for both air-water and oil-water interface systems. Hydronium tends to reside in the topmost layer of the interface, while hydroxide with a slightly stronger interfacial stabilization free energy is enriched in the deeper interfacial layer. This double-layer distribution may help to understand the longstanding controversy about the interfacial acid-base nature.

Water interfaces play a crucial role in both natural sciences and engineering applications due to providing fundamental heterogeneous environments.¹⁻³ The preferential accumulation of water self-ions at these interfaces, namely hydroxide (OH^-) and hydronium (H_3O^+), can impact both interfacial properties^{4,5} and chemical reaction processes,⁵⁻⁹ and has been widely investigated. Nevertheless, the propensity of self-ions enriching at air-water and oil-water interfaces continues to be an open question due to opposite findings from these previous studies.¹⁰⁻²²

For example, the macroscopic experiments measured the negative zeta potential of air bubbles²³⁻²⁶ and oil droplets^{25,27,28} in water and inferred the enrichment of OH^- at the air(oil)-water interfaces considering that OH^- is the only anionic source in pure water. The second harmonic generation study also provided spectroscopic

evidence for the adsorption of OH^- at the oil-water interface.¹⁷ However, further spectroscopic measurements observed the interfacial enhancement of H_3O^+ .^{10,21,29} Similarly, plenty of microscopic simulations also obtained conflicting conclusions on the interfacial excess of self-ions.^{15,16,18,19,30,31}

Our recent deep potential molecular dynamics (DPMD) simulations on ionic distribution at the air-water interface³² provide a possible explanation for the inconsistency of these conclusions. We found evidence for an interfacial double-layer distribution of water self-ions. In this distribution, H_3O^+ predominantly occupies the top layer of the interface, while OH^- is enriched in the deeper layer below that of H_3O^+ . Compared to H_3O^+ , OH^- has a more negative free energy of interfacial stabilization and accordingly a higher interfacial concentration, leading to

negatively charged interfaces and negative zeta potential. These results are consistent with the macroscopic detection and do not contradict microscopic observation, as the previous conflicting results may be caused by measuring at different or ambiguous interfacial depths. However, it is important to note that our previous work performed separate simulations for OH^- and H_3O^+ , without considering their origins and recombination at the interface. Therefore, in this work, we performed further investigation with the corresponding consideration to validate the observation of the double-layer distribution.

Technically, it is pretty demanding to simulate the water autoionization reaction of forming OH^- and H_3O^+ , and its reverse process of ionic recombination. Although many mechanistic studies on these processes in bulk water have been conducted for decades,³³⁻⁴¹ accurately simulating the free energy profiles to match experimental results remains a challenge. This is primarily because water autoionization is an exceedingly rare event. Here, we utilized the recently developed on-the-fly probability enhanced sampling (OPES) method^{42,43} with a set of Voronoi collective variables (CVs)⁴⁴⁻⁴⁶ to sample this rare event efficiently. Additionally, to get the converged free energy through enhanced sampling, the timescale of nanoseconds is usually needed, which is beyond the capabilities of conventional *ab initio* MD (AIMD) simulations. Therefore, we employed neural network potential models with approximate M06-2X⁴⁷ accuracy to drive MD simulations. Armed with these state-of-the-art methods, we obtained the free energy of water autoionization in quantitative agreement with experimental observations. Most significantly, the present deep-going investigation confirms the phenomenon of the ionic double-layer distribution at the air-water interface with a full consideration of water autoionization and its reverse recombination processes. In addition, we further extended our study to the oil-water interface, and we found a similar double-layer distribution of water self-ions.

Before discussing ionic preferences at interfaces, it is important to validate the feasibility of our methodologies for accurately describing water autoionization and its reverse process. We first need an efficient potential with an accuracy approaching hybrid meta-GGA functional M06-2X.⁴⁷ We chose to learn the energies and forces of the M06-2X functional because of its reported accuracy for modeling liquid water.⁴⁸ To expedite this step, we initially trained a deep Kohn-Sham (DeePKS) model⁴⁹⁻⁵¹ with the precision of M06-2X, which saves approximately nine times more time than the regular M06-2X calculations. Then, we trained a deep potential (DP) model to closely match the accuracy of the DeePKS model, i.e., the trained DP model would have an approximate M06-2X accuracy.

Finally, molecular dynamics simulations were driven by the DP model (DPMD),^{52,53} which offers a time-saving of more than five orders of magnitude when compared to the AIMD simulations directly using the M06-2X.

In the simulation, to efficiently sample the rare event of water autoionization, we employed the OPES method. In this way, appropriate CVs must be defined. To depict both the production of OH^- and H_3O^+ by water autoionization and the diffusion of these self-ions through the Grotthuss mechanism,^{32,54,55} we tessellated the space into Voronoi polyhedra centered on all oxygen atoms and summed up the atomic charges within each polyhedron, that can enable us to automatically identify charge defects of OH^- and H_3O^+ without a priori knowledge, and accordingly designed CVs, self-ion number \mathbf{s}_a

$$\mathbf{s}_a = \sum_{i=1}^{\text{Num}_O} \delta_i^2, \quad (1)$$

self-ion distance \mathbf{s}_t

$$\mathbf{s}_t = - \sum_{i=1}^{\text{Num}_O} \sum_{j>i}^{\text{Num}_O} r_{i,j} \delta_i \delta_j, \quad (2)$$

and its variant \mathbf{s}'_t

$$\mathbf{s}'_t = \begin{cases} \log(\mathbf{s}_t + \epsilon), & 0 \leq \mathbf{s}_t < 1, \\ \mathbf{s}_t - 1 + \log(1 + \epsilon), & \mathbf{s}_t \geq 1, \end{cases} \quad (3)$$

to distinguish the water autoionization process. The charge defect of the i th Voronoi center (O atom) is denoted by δ_i , with values 0, 1, and -1 for H_2O , H_3O^+ , and OH^- respectively. Distance between two Voronoi centers is represented by $r_{i,j}$. Consequently, the CV \mathbf{s}_a signifies the number of H_3O^+ and OH^- ions resulting from water autoionization, while the CV \mathbf{s}_t indicates the distance between two ions. However, the CV \mathbf{s}_t struggles to differentiate between pure water and transition states, so we introduced its logarithmic variant CV \mathbf{s}'_t to address this issue. More details of CVs and other simulation settings are provided in the Supporting Information (SI).

Based on the DPMD simulations, we calculated the free energy surface (FES) as a function of the two defined CVs (\mathbf{s}_a and \mathbf{s}'_t). As shown in Fig. 1a, a deep well is located at $\mathbf{s}_a = 0$ and $\mathbf{s}'_t = -3.6$ which presents the neutral water molecules bonded with the hydrogen bonds, namely, the reactant of water autoionization reaction. We also observed a shallow well at $\mathbf{s}_a = 1.3$ and $\mathbf{s}'_t = 4.8$ corresponding to the autoionization products (OH^- and H_3O^+) separated by a water wire with a length of ~ 6 Å that indicates the metastability of self-ions pair. We further identified the optimal path connecting the two wells and marked it with the white dot line in Fig. 1a,

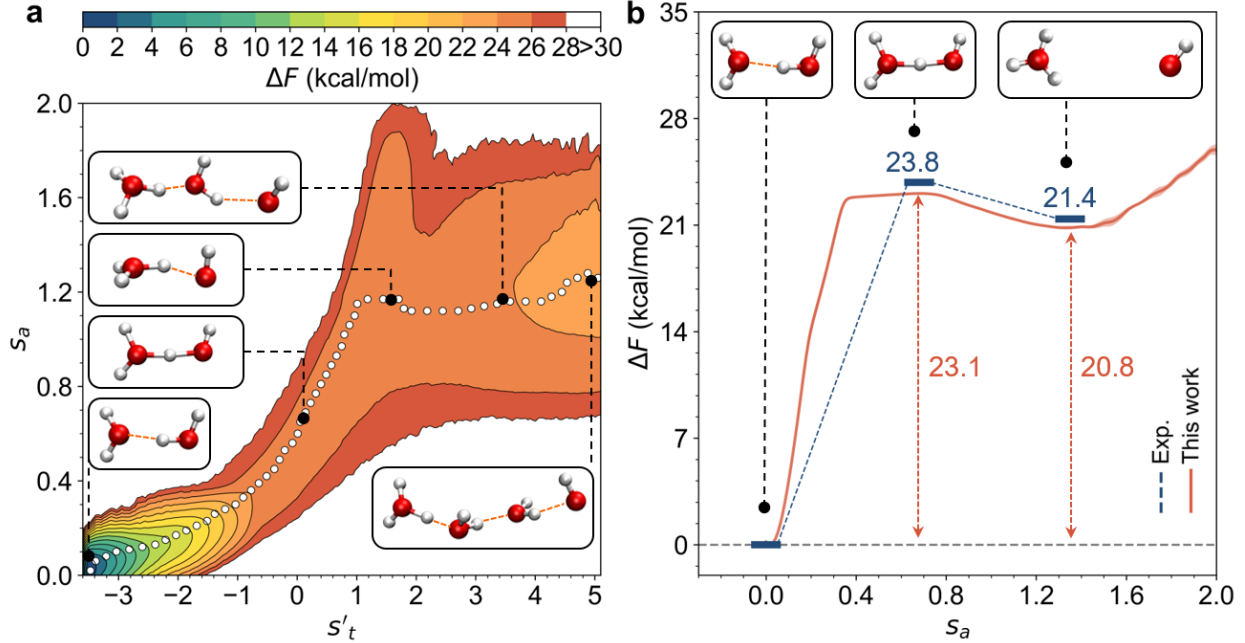


Figure 1: **Free energy surface of water autoionization.** **a.** Two-dimensional FES as a function of the ionic distance variant s'_t and the ionic number s_a , where the minimum free energy path of autoionization is represented by the white dot line. Key structures along the potential optimal pathway of water autoionization are provided, in which surrounding water molecules are hidden. Color code: hydrogen, white; oxygen, red. **b.** One-dimensional projection of the FES along the ionic number coordinate s_a . Experimental values are also provided for comparison.

accompanied by the key structures along the path. It is revealed that the water autoionization process occurs via the concerted transfer of multiple protons along the water wire, which follows the Grotthuss mechanism,^{38,39} and eventually forms the well-separated OH^- and H_3O^+ ions.

By projecting the FES along the self-ion number CV, s_a , we got a one-dimensional free energy curve (Fig. 1b) to clearly show the free energy change of the reaction process. From Fig. 1b, the activation free energy (ΔF^\ddagger) and the reaction free energy (ΔF°) of the water autoionization reaction are estimated as 23.1 and 20.8 kcal/mol, respectively, which are in good agreement with the experimental measurements ($\Delta F^\ddagger = 23.8$ kcal/mol, $\Delta F^\circ = 21.4$ kcal/mol).^{33,35,36} The reverse process—recombination of self-ions, may occur by overcoming a low barrier of approximately 2.3 kcal/mol, which is close to the proton transfer barrier (2.4 kcal/mol) observed in NMR experiments.⁵⁶ These results demonstrate the accuracy of our simulations in characterizing the potential energy landscape of water autoionization.

Having validated the accuracy of the methodologies, we shifted our focus to investigating the distribution preference of water self-ions near the air-water and oil-water interfaces. To this end, in simulations we introduced two

new CVs, s_{zn}

$$s_{zn} = \sum_{i=1}^{\text{Num}_O} \delta z_i \delta_i^2 \quad (\text{for } \delta_i < 0), \quad (4)$$

and s_{zp}

$$s_{zp} = \sum_{i=1}^{\text{Num}_O} \delta z_i \delta_i^2 \quad (\text{for } \delta_i > 0), \quad (5)$$

where δz indicates the relative coordinate along the z -axis. Thus, the CVs s_{zn} and s_{zp} can describe depths of OH^- and H_3O^+ relative to the interfaces, respectively. The free energy curves of OH^- and H_3O^+ distribution as functions of s_{zn} and s_{zp} , respectively, were calculated and plotted in Fig. 2, where we took the position of the interface as the zero point of s_{zn} and s_{zp} for a better understanding of the relative locations to the interface. In this work, the interface of the air-water system is defined to be the surface where the water density is half of its bulk value, and the interface of the oil-water system is set as the surface with the minimum density between the oil and water phases considering the hydrophobicity of oil. Negative values and positive values of s_{zn} and s_{zp} denote the water phase and air (or oil) phase, respectively.

The FES results shown in Fig. 2 strongly support the double-layer distribution of water self-ions near the in-

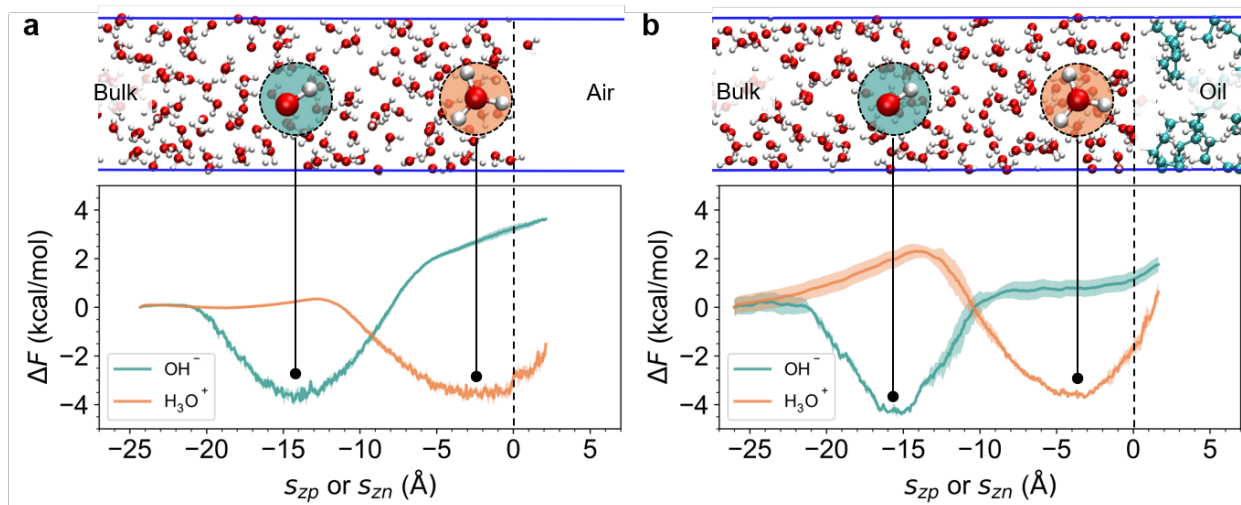


Figure 2: **Double-layer distribution of water self-ions near the interface.** One-dimensional free energy curves of ionic preference in **a.** the air-water interface and **b.** the oil-water interface are depicted below the corresponding schematic diagrams. Based on the value of CVs s_{zn} and s_{zp} , the normal distances to the reference surface are negative on the liquid side, zero at the surface, and positive on the air or oil side. In the schematic diagrams, particular emphasis is placed on highlighting the distinct preferential distribution of OH^- and H_3O^+ ions near the interface. Carbon atoms are visually represented using green sphere models.

terface reported in our previous study.³² For both cases (the air-water and oil-water systems), we can clearly see two free energy wells located at different depths near the interface, which represent the preferential locations of OH^- and H_3O^+ , respectively. The free energy well of H_3O^+ spans the region of 0-1 nm below the interface, with the minimum ($-3.8/-3.7$ kcal/mol) located at $s_{zp} = -2/-3\text{\AA}$ for the air-water/oil-water system; the free energy well of OH^- appears in a deeper layer spanning the region of 1-2 nm below the interface, and the corresponding minimum has a free energy of $-3.9/-4.4$ kcal/mol (air-water/oil-water). (Note, the reported free energies here are the relative values to the bulk.)

Fig. 2 also shows that OH^- needs to surpass a barrier of ~ 7 (~ 5) kcal/mol to reside in the location predominantly occupied by H_3O^+ in the air-water (oil-water) system, and H_3O^+ needs to overcome a barrier of around ~ 4 (~ 6) kcal/mol to approach the position mostly filled by OH^- in the air-water (oil-water) system. These further support the stability of the double-layer distribution of self-ions near the interfaces from a dynamic aspect. The current simulation results show that the energy well of OH^- near the interface is slightly deeper than that of H_3O^+ , with differences of 0.1 and 0.7 kcal/mol in the air-water interface and oil-water interface, respectively. This aligns with the earlier work, which, using different potential (the deep potential learned from SCAN functional⁵⁷) and sampling methods, yielded a difference of 0.3 kcal/mol between

the interfacial stabilization energies of OH^- and H_3O^+ .³² Based on the observed stronger interfacial propensity of OH^- than H_3O^+ , it is reasonably postulated that the measured experimentally negative zeta potential^{23–28,58} may arise from more accumulation of OH^- than H_3O^+ near the water interface.

Different experimental techniques may probe varying depths of the interfacial region and therefore conclude differently.^{21,32,59–61} For instance, original vibrational sum frequency generation (vSFG) techniques, which provide information solely in the noncentrosymmetric region,⁶² may not effectively detect the distribution of OH^- in the deeper layer of the interface due to its random orientation.^{63–66} The adsorption of H_3O^+ at the top layer in a relatively orderly arrangement exhibits distinct spectroscopic signatures compared to the water, and therefore, the interfacial propensity of the proton has been revealed by preceding microscopic studies.^{10,15–19,21,29,31} This microscopic observation is also confirmed by the current simulations.

Notably, recent high-level heterodyne-detected vSFG results may corroborate our simulation results, which provided evidence of H_3O^+ accumulation at the outermost surface and OH^- enrichment in the subsurface layer.⁶⁷ Since their system consists primarily of electrolyte solutions, addressing the challenge of detecting rare events such as autoionization and ionic preference on a pure water surface is desired in future experimental studies.

In addition, it is noticed that OH^- has a remarkably more negative interfacial stabilization free energy in the oil-water interface than in the air-water interface, i.e., OH^- has a stronger propensity in the oil-water interface, on the contrary, the propensity of H_3O^+ in the interface is similar in the two cases. It can be due to more pronounced asymmetry and amphiphathy in molecular charge distribution in OH^- .⁶⁸ This observation could account for the more frequent detection of negative zeta potentials in cases involving oil droplets.^{25,27,28,58}

In summary, with enhanced-sampling techniques that can efficiently sample water autoionization processes and describe well ionic diffusion and recombination, we demonstrated the interfacial double-layer distribution of OH^- and H_3O^+ in both air-water and oil-water systems by deep potential molecular dynamics simulations, where OH^- with stronger interfacial stabilization free energy accumulates more than H_3O^+ . Consequently, this stable double-layer distribution may provide a qualitatively self-consistent interpretation, reconciling previous macroscopic and microscopic studies on the ionic distribution near water interfaces. This research also offers valuable insights that contribute potentially to the field of engineering applications in the air-water⁶⁹ and oil-water interfaces.^{70,71}

Data and Software Availability

The simulation and visualization packages used to perform the calculations are freely available. The input files needed to reproduce the research are available at <https://github.com/Zhang-pchao/OilWaterInterface>.

Supporting Information Available

Potential model generation, including construction of training datasets, density functional theory calculation, DeePKS model, and DP model training. Molecular dynamics, including MD simulation for the training dataset generation, and DPMD simulation for studying the autoionization and the double-layer distribution. Enhanced sampling settings, including bias potential, definition of collective variables, and free energy calculation. Error distribution on the testing dataset, uncertainty of atomic force predictions, one-dimensional FES and other details (PDF)

Author contributions

P.Z. and A.T.G. carried out the testing of the enhanced sampling technique on water autoionization. P.Z. conducted the simulation workflow and performed data analysis. X.X. provided supervision throughout the project stages. The initial draft of the manuscript was prepared by P.Z.,

and all authors participated in editing and reviewing the final version.

Declaration of Competing Interest

The authors declare no competing financial interest.

Acknowledgments

This work was partially supported by the National Natural Science Foundation of China under Grant Nos. [21973053, 11988102]. The authors acknowledge the valuable discussions with Professor Michele Parrinello. Computational resources were provided by the High Performance Computing (HPC) platform at Tsinghua University and the HPC Franklin at Fondazione Istituto Italiano di Tecnologia.

References

- [1] Ruiz-Lopez, M. F.; Francisco, J. S.; Martins-Costa, M. T.; Anglada, J. M. Molecular reactions at aqueous interfaces. *Nature Reviews Chemistry* **2020**, *4*, 459–475.
- [2] Wei, Z.; Li, Y.; Cooks, R. G.; Yan, X. Accelerated reaction kinetics in microdroplets: Overview and recent developments. *Annual Review of Physical Chemistry* **2020**, *71*, 31–51.
- [3] Björneholm, O.; Hansen, M. H.; Hodgson, A.; Liu, L.-M.; Limmer, D. T.; Michaelides, A.; Pedevilla, P.; Rossmeisl, J.; Shen, H.; Tocci, G.; others Water at interfaces. *Chemical reviews* **2016**, *116*, 7698–7726.
- [4] Chamberlayne, C. F.; Zare, R. N. Simple model for the electric field and spatial distribution of ions in a microdroplet. *The Journal of chemical physics* **2020**, *152*.
- [5] Martins-Costa, M. T.; Ruiz-López, M. F. Electrostatics and chemical reactivity at the air–water interface. *Journal of the American Chemical Society* **2023**, *145*, 1400–1406.
- [6] Li, Y.; Chen, Y.-X.; Liu, Z.-F. $\text{OH}^- \cdots \text{Au}$ Hydrogen Bond and Its Effect on the Oxygen Reduction Reaction on Au (100) in Alkaline Media. *The Journal of Physical Chemistry Letters* **2022**, *13*, 9035–9043.
- [7] Zhong, G.; Cheng, T.; Shah, A. H.; Wan, C.; Huang, Z.; Wang, S.; Leng, T.; Huang, Y.; Goddard III, W. A.; Duan, X. Determining the hydronium pK_a at platinum surfaces and the effect on pH-dependent hydrogen evolution reaction kinetics. *Proceedings of the National Academy of Sciences* **2022**, *119*, e2208187119.
- [8] Lee, J. K.; Walker, K. L.; Han, H. S.; Kang, J.; Prinz, F. B.; Waymouth, R. M.; Nam, H. G.; Zare, R. N. Spontaneous generation of hydrogen peroxide from aqueous microdroplets. *Proceedings of the National Academy of Sciences* **2019**, *116*, 19294–19298.
- [9] Song, X.; Basheer, C.; Zare, R. N. Making ammonia from nitrogen and water microdroplets. *Proceedings of the National Academy of Sciences* **2023**, *120*, e2301206120.
- [10] Vácha, R.; Buch, V.; Milet, A.; Devlin, J. P.; Jungwirth, P. Autoionization at the surface of neat water: is the top layer pH neutral, basic, or acidic? *Physical Chemistry Chemical Physics* **2007**, *9*, 4736–4747.
- [11] Buch, V.; Milet, A.; Vácha, R.; Jungwirth, P.; Devlin, J. P. Water surface is acidic. *Proceedings of the National Academy of Sciences* **2007**, *104*, 7342–7347.
- [12] Beattie, J. K.; Djerdjev, A. M.; Warr, G. G. The surface of neat water is basic. *Faraday discussions* **2009**, *141*, 31–39.
- [13] Mishra, H.; Enami, S.; Nielsen, R. J.; Stewart, L. A.; Hoffmann, M. R.; Goddard III, W. A.; Colussi, A. J. Brønsted basicity of the air–water interface. *Proceedings of the National Academy of Sciences* **2012**, *109*, 18679–18683.
- [14] Saykally, R. J. Two sides of the acid–base story. *Nature chemistry* **2013**, *5*, 82–84.
- [15] Hub, J. S.; Wolf, M. G.; Caleman, C.; van Maaren, P. J.; Groenhof, G.; van der Spoel, D. Thermodynamics of hydronium and hydroxide surface solvation. *Chemical Science* **2014**, *5*, 1745–1749.
- [16] Baer, M. D.; Kuo, I.-F. W.; Tobias, D. J.; Mundy, C. J. Toward a unified picture of the water self-ions at the air–water interface: A density functional theory perspective. *The Journal of Physical Chemistry B* **2014**, *118*, 8364–8372.

- [17] Fang, H.; Wu, W.; Sang, Y.; Chen, S.; Zhu, X.; Zhang, L.; Niu, Y.; Gan, W. Evidence of the adsorption of hydroxide ion at hexadecane/water interface from second harmonic generation study. *Rsc Advances* **2015**, *5*, 23578–23585.
- [18] Tse, Y.-L. S.; Chen, C.; Lindberg, G. E.; Kumar, R.; Voth, G. A. Propensity of hydrated excess protons and hydroxide anions for the air–water interface. *Journal of the American Chemical Society* **2015**, *137*, 12610–12616.
- [19] Bai, C.; Herzfeld, J. Surface propensities of the self-ions of water. *ACS central science* **2016**, *2*, 225–231.
- [20] Mamatkulov, S. I.; Allolio, C.; Netz, R. R.; Bonthuis, D. J. Orientation-induced adsorption of hydrated protons at the air–water interface. *Angewandte Chemie International Edition* **2017**, *56*, 15846–15851.
- [21] Das, S.; Imoto, S.; Sun, S.; Nagata, Y.; Backus, E. H.; Bonn, M. Nature of excess hydrated proton at the water–air interface. *Journal of the American Chemical Society* **2019**, *142*, 945–952.
- [22] Colussi, A. J.; Enami, S.; Ishizuka, S. Hydronium ion acidity above and below the Interface of aqueous microdroplets. *ACS Earth and Space Chemistry* **2021**, *5*, 2341–2346.
- [23] Quincke, G. Ueber die Fortführung materieller Theilchen durch strömende Elektrizität. *Annalen der Physik* **1861**, *189*, 513–598.
- [24] Graciaa, A.; Morel, G.; Saulner, P.; Lachaise, J.; Schechter, R. The ζ -potential of gas bubbles. *Journal of Colloid and Interface Science* **1995**, *172*, 131–136.
- [25] Creux, P.; Lachaise, J.; Graciaa, A.; Beattie, J. K.; Djerdjev, A. M. Strong specific hydroxide ion binding at the pristine oil/water and air/water interfaces. *The Journal of Physical Chemistry B* **2009**, *113*, 14146–14150.
- [26] Creux, P.; Lachaise, J.; Graciaa, A.; Beattie, J. K. Specific cation effects at the hydroxide-charged air/water interface. *The Journal of Physical Chemistry C* **2007**, *111*, 3753–3755.
- [27] Marinova, K.; Alargova, R.; Denkov, N.; Velev, O.; Petsev, D.; Ivanov, I.; Borwankar, R. Charging of oil-water interfaces due to spontaneous adsorption of hydroxyl ions. *Langmuir* **1996**, *12*, 2045–2051.
- [28] Beattie, J. K.; Djerdjev, A. M. The pristine oil/water interface: Surfactant-free hydroxide-charged emulsions. *Angewandte Chemie International Edition* **2004**, *43*, 3568–3571.
- [29] Petersen, P. B.; Saykally, R. J. Evidence for an enhanced hydronium concentration at the liquid water surface. *The Journal of Physical Chemistry B* **2005**, *109*, 7976–7980.
- [30] de la Puente, M.; Laage, D. How the Acidity of Water Droplets and Films Is Controlled by the Air–Water Interface. *Journal of the American Chemical Society* **2023**.
- [31] Mundy, C. J.; Kuo, I.-F. W.; Tuckerman, M. E.; Lee, H.-S.; Tobias, D. J. Hydroxide anion at the air–water interface. *Chemical Physics Letters* **2009**, *481*, 2–8.
- [32] Zhang, P.; Feng, M.; Xu, X. Double-layer distribution of hydronium and hydroxide ions in the air-water interface. *ACS Physical Chemistry Au* **2024**.
- [33] Eigen, M.; De Maeyer, L. Untersuchungen über die Kinetik der Neutralisation. I. *Zeitschrift für Elektrochemie, Berichte der Bunsengesellschaft für physikalische Chemie* **1955**, *59*, 986–993.
- [34] Eigen, M.; De Maeyer, L. Self-dissociation and protonic charge transport in water and. *Proceedings of the Royal Society of London. Series A. Mathematical and Physical Sciences* **1958**, *247*, 505–533.
- [35] Åqvist, J.; Warshel, A. Simulation of enzyme reactions using valence bond force fields and other hybrid quantum/classical approaches. *Chemical reviews* **1993**, *93*, 2523–2544.
- [36] Trout, B. L.; Parrinello, M. The dissociation mechanism of H₂O in water studied by first-principles molecular dynamics. *Chemical physics letters* **1998**, *288*, 343–347.
- [37] Geissler, P. L.; Dellago, C.; Chandler, D.; Hutter, J.; Parrinello, M. Autoionization in liquid water. *Science* **2001**, *291*, 2121–2124.
- [38] Hassanali, A.; Prakash, M. K.; Eshet, H.; Parrinello, M. On the recombination of hydronium and hydroxide ions in water. *Proceedings of the National Academy of Sciences* **2011**, *108*, 20410–20415.
- [39] Moqadam, M.; Lervik, A.; Riccardi, E.; Venkatraman, V.; Alsborg, B. K.; van Erp, T. S. Local initiation conditions for water autoionization. *Proceedings of the National Academy of Sciences* **2018**, *115*, E4569–E4576.
- [40] Liu, L.; Tian, Y.; Yang, X.; Liu, C. Mechanistic Insights into Water Autoionization through Metadynamics Simulation Enhanced by Machine Learning. *Physical Review Letters* **2023**, *131*, 158001.
- [41] Calegari Andrade, M.; Car, R.; Selloni, A. Probing the self-ionization of liquid water with ab initio deep potential molecular dynamics. *Proceedings of the National Academy of Sciences* **2023**, *120*, e2302468120.
- [42] Invernizzi, M.; Parrinello, M. Rethinking metadynamics: From bias potentials to probability distributions. *The journal of physical chemistry letters* **2020**, *11*, 2731–2736.
- [43] Invernizzi, M.; Parrinello, M. Exploration vs convergence speed in adaptive-bias enhanced sampling. *Journal of Chemical Theory and Computation* **2022**, *18*, 3988–3996.
- [44] Grifoni, E.; Piccini, G.; Parrinello, M. Microscopic description of acid–base equilibrium. *Proceedings of the National Academy of Sciences* **2019**, *116*, 4054–4057.
- [45] Grifoni, E.; Piccini, G.; Parrinello, M. Tautomeric equilibrium in condensed phases. *Journal of Chemical Theory and Computation* **2020**, *16*, 6027–6031.
- [46] Zhang, P.; Gardini, A. T.; Xu, X.; Parrinello, M. Intramolecular and water mediated tautomerism of solvated glycine. *Journal of Chemical Information and Modeling* **2024**.
- [47] Zhao, Y.; Truhlar, D. G. The M06 suite of density functionals for main group thermochemistry, thermochemical kinetics, noncovalent interactions, excited states, and transition elements: two new functionals and systematic testing of four M06-class functionals and 12 other functionals. *Theoretical chemistry accounts* **2008**, *120*, 215–241.
- [48] Villard, J.; Bircher, M. P.; Rothlisberger, U. Structure and dynamics of liquid water from ab initio simulations: Adding Minnesota density functionals to Jacob’s ladder. *Chemical Science* **2024**.
- [49] Chen, Y.; Zhang, L.; Wang, H.; E, W. DeePKS: A comprehensive data-driven approach toward chemically accurate density functional theory. *Journal of Chemical Theory and Computation* **2020**, *17*, 170–181.
- [50] Chen, Y.; Zhang, L.; Wang, H.; Weinan, E. DeePKS-kit: A package for developing machine learning-based chemically accurate energy and density functional models. *Computer Physics Communications* **2023**, *282*, 108520.
- [51] Li, W.; Ou, Q.; Chen, Y.; Cao, Y.; Liu, R.; Zhang, C.; Zheng, D.; Cai, C.; Wu, X.; Wang, H.; others DeePKS+ABACUS as a Bridge between Expensive Quantum Mechanical Models and Machine Learning Potentials. *The Journal of Physical Chemistry A* **2022**, *126*, 9154–9164.
- [52] Wang, H.; Zhang, L.; Han, J.; E, W. DeePMD-kit: A deep learning package for many-body potential energy representation and molecular dynamics. *Computer Physics Communications* **2018**, *228*, 178–184.
- [53] Zeng, J.; Zhang, D.; Lu, D.; Mo, P.; Li, Z.; Chen, Y.; Rynik, M.; Huang, L.; Li, Z.; Shi, S.; others DeePMD-kit v2: A software package for deep potential models. *The Journal of Chemical Physics* **2023**, *159*.
- [54] de Grotthuss, C. J. T. Mémoire sur la Décomposition de l’Eau et des Corps qu’elle Tient en Dissolution à l’Aide de l’Électricité Galvanique. *Ann. Chim.* **1806**, 54–74.
- [55] Marx, D. Proton transfer 200 years after von Grotthuss: Insights from *ab initio* simulations. *ChemPhysChem* **2006**, *7*, 1848–1870.
- [56] Luz, Z.; Meiboom, S. The activation energies of proton transfer reactions in water. *Journal of the American Chemical Society* **1964**, *86*, 4768–4769.
- [57] Sun, J.; Ruzsinszky, A.; Perdew, J. P. Strongly constrained and appropriately normed semilocal density functional. *Physical review letters* **2015**, *115*, 036402.
- [58] Agmon, N.; Bakker, H. J.; Campen, R. K.; Henchman, R. H.; Pohl, P.; Roke, S.; Thaömer, M.; Hassanali, A. Protons and hydroxide ions in aqueous systems. *Chemical reviews* **2016**, *116*, 7642–7672.
- [59] Du, Q.; Freysz, E.; Shen, Y. R. Vibrational spectra of water molecules at quartz/water interfaces. *Physical Review Letters* **1994**, *72*, 238.
- [60] Inoue, K.-i.; Nihonyanagi, S.; Singh, P. C.; Yamaguchi, S.; Tahara, T. 2D heterodyne-detected sum frequency generation study on the ultrafast vibrational dynamics of H₂O and HOD water at charged interfaces. *The Journal of Chemical Physics* **2015**, *142*.
- [61] Montenegro, A.; Dutta, C.; Mammetskuliev, M.; Shi, H.; Hou, B.; Bhattacharyya, D.; Zhao, B.; Cronin, S. B.; Benderskii, A. V. Asymmetric response of interfacial water to applied electric fields. *Nature* **2021**, *594*, 62–65.
- [62] Ishiyama, T.; Morita, A. Computational Analysis of Vibrational Sum Frequency Generation Spectroscopy. *Annu. Rev. Phys. Chem.* **2017**, *68*, 355–377.
- [63] Somorjai, G. A.; Park, J. Y. Molecular surface chemistry by metal single crystals and nanoparticles from vacuum to high pressure. *Chemical Society Reviews* **2008**, *37*, 2155–2162.
- [64] Zaera, F. Probing liquid/solid interfaces at the molecular level. *Chemical reviews* **2012**, *112*, 2920–2986.
- [65] Tang, F.; Ohto, T.; Sun, S.; Rouxel, J. R.; Imoto, S.; Backus, E. H.; Mukamel, S.; Bonn, M.; Nagata, Y. Molecular structure and modeling of water–air and ice–air interfaces monitored by sum-frequency generation. *Chemical reviews* **2020**, *120*, 3633–3667.
- [66] Sakunkaewkasem, S.; Deleon, D.; Choi, Y.; Tran, H.-V.; Marquez, M. D.; Baldelli, S.; Lee, T. R. Sum frequency generation spectroscopy of fluorinated organic material-based interfaces: a tutorial review. *Analyst* **2023**, *148*, 2901–2920.

- [67] Litman, Y.; Chiang, K.-Y.; Seki, T.; Nagata, Y.; Bonn, M. Surface stratification determines the interfacial water structure of simple electrolyte solutions. *Nature Chemistry* **2024**, 1–7.
- [68] Kudin, K. N.; Car, R. Why are water-hydrophobic interfaces charged? *Journal of the American Chemical Society* **2008**, *130*, 3915–3919.
- [69] Kusaka, R.; Nihonyanagi, S.; Tahara, T. The photochemical reaction of phenol becomes ultrafast at the air–water interface. *Nature Chemistry* **2021**, *13*, 306–311.
- [70] Tian, Y.-M.; Silva, W.; Gschwind, R. M.; König, B. Accelerated photochemical reactions at oil-water interface exploiting melting point depression. *Science* **2024**, *383*, 750–756.
- [71] Chen, X.; Xia, Y.; Wu, Y.; Xu, Y.; Jia, X.; Zare, R. N.; Wang, F. Sprayed Oil–Water Microdroplets as a Hydrogen Source. *Journal of the American Chemical Society* **2024**,

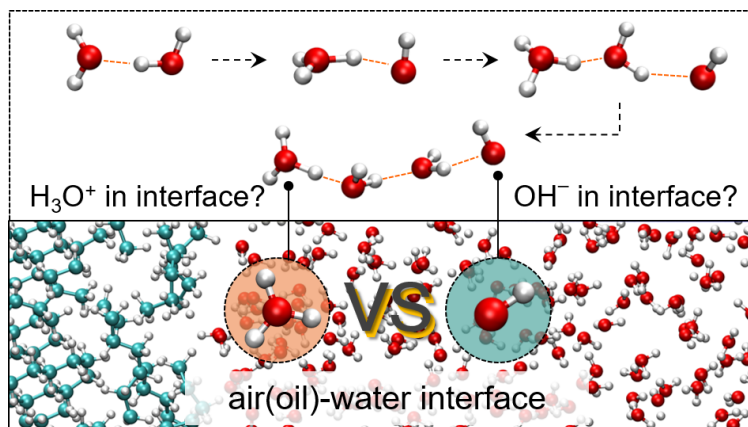


Table of contents (TOC)